Planar laser-induced fluorescence of CF_2 in O_2/CF_4 and O_2/C_2F_6 chamber-cleaning plasmas: Spatial uniformity and comparison to electrical measurements

Kristen L. Steffens[a)] and Mark A. Sobolewski
National Institute of Standards and Technology, Gaithersburg, Maryland 20899

Planar laser-induced fluorescence (PLIF) measurements were made to determine two-dimensional spatial maps of CF_2 density as an indicator of chemical uniformity in 92% CF_4/O_2 and 50% C_2F_6/O_2 chamber-cleaning plasmas at pressures between 13.3 Pa (100 mTorr) and 133.3 Pa (1000 mTorr). Measurements were also made of broadband optical emission and of discharge current, voltage and power. All measurements were made in a Gaseous Electronics Conference Reference Cell, a capacitively coupled, parallel-plate platform designed to facilitate comparison of results among laboratories. The CF_2 PLIF and emission results were found to correlate with discharge current and voltage measurements. Together, these optical and electrical measurements provide insight into the optimization of chamber-cleaning processes and reactors, suggest new methods of monitoring plasma uniformity, and identify important spatial effects which should be included in computer simulations.   [S0734-2101(99)02602-0]

I. INTRODUCTION

During the plasma-enhanced chemical vapor deposition (PECVD) of Si, SiO_2 and Si_3N_4 films, deposition occurs not only on the substrate as desired, but also on all interior reactor surfaces. If not removed, these films accumulate, flake off and cause critical particulate problems during the PECVD process. Perfluorocarbon (PFC) plasmas, which are extensively used in the semiconductor industry for etching of Si, SiO_2 and Si_3N_4, are used as an efficient *in situ* method for removing these films from reactor surfaces. To be feasible for commercial use, chamber cleaning must be rapid and efficient and must minimize the emission of PFCs, which contribute to the greenhouse effect.[1] These requirements become even more important as industry increasingly adopts processes in which cleaning procedures are performed after each deposition.[2] To obtain optimal results, the applied rf power must be efficiently transferred to plasma electrons, since collisions involving energetic electrons produce the chemically reactive species necessary for chamber cleaning. Also, the spatial distribution of the chemically reactive species in the plasma should be tailored so that the species are readily transported to surfaces which are most in need of cleaning. Studies of the power absorption mechanisms and spatial uniformity of chamber-cleaning plasmas are therefore of critical interest, since the information and understanding provided by such studies could improve chamber-cleaning processes and equipment.

In previous studies of NF_3/Ar, CF_4/O_2, and C_2F_6/O_2 chamber-cleaning plasmas, power losses in rf circuitry[3–5] and the mechanisms of power absorption within the discharge[5] have been investigated. In those studies, the power delivered to the plasma and the electrical impedance of the plasma were identified as important parameters.

Changes in the plasma power and plasma impedance were correlated to changes in etch rates,[3,4] optical emission intensities,[3,5] and the destruction efficiency of feed gases.[6] Visually observed changes in the spatial uniformity of chamber cleaning plasmas were also reported and correlated with plasma impedance,[5] but plasma spatial uniformity was not the major subject of that work. The spatial uniformity of chamber-cleaning plasmas, and in particular the spatial distribution of chemical species within the plasma, are important subjects that merit more detailed, quantitative study.

In this study, the spatial uniformity of O_2/CF_4 and O_2/C_2F_6 chamber-cleaning plasmas as a function of pressure, gas mixture and power was characterized using two optical techniques: planar laser induced fluorescence (PLIF) and optical emission. Using PLIF, the two-dimensional (2D) spatial density of the CF_2 radical was monitored. The CF_2 radical is an important species in the chemical reactions that control the concentration of the fluorine radical,[7] which is believed to be the active chemical etchant.[8] As such, CF_2 is a useful marker of chemical uniformity in the plasma. Two-dimensional broadband optical emission measurements provided complementary information, indicating where in the plasma excited species are formed. Measurements of discharge electrical characteristics were also performed. Correlations between the PLIF, emission, and electrical measurements were observed. These correlations help explain the observed variations in plasma uniformity, identify important spatial effects which should be included in computer simulations, and suggest new methods of monitoring and optimizing chamber-cleaning plasmas.

II. EXPERIMENT

Experiments were conducted in a Gaseous Electronics Conference (GEC) Reference Reactor.[9,10] The reactor, shown in Fig. 1(a), is a parallel-plate, capacitively coupled
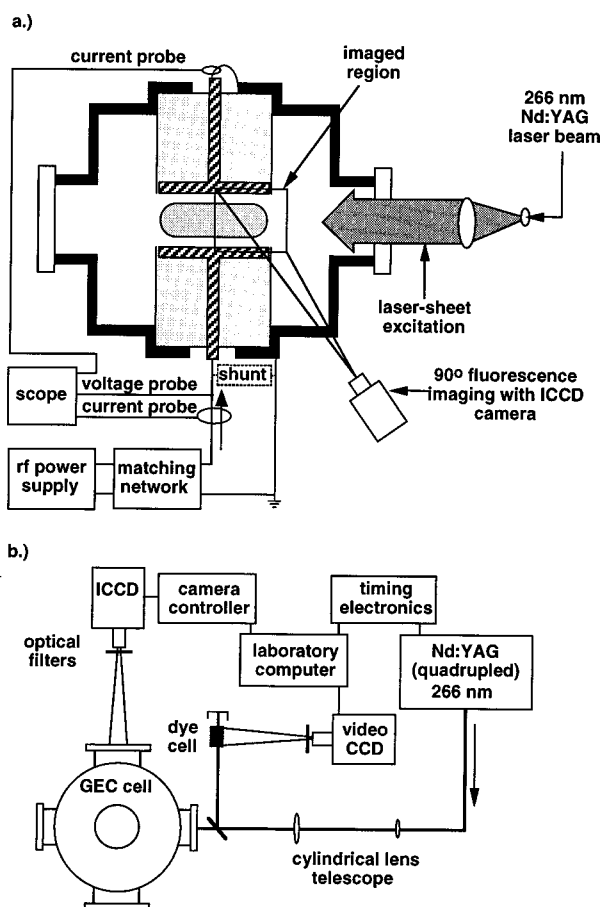
a.)

b.)

FIG. 1. Experimental schematic: (a) Side view of GEC Reference Cell, including diagram of electrical probes and PLIF details, (b) Top view of GEC reference cell, illustrating PLIF detection.

radio-frequency (rf) discharge reactor with 10.2 cm diam, water-cooled, aluminum electrodes spaced by 2.25 cm. Each electrode is surrounded by a ground shield. The lower electrode is powered and the upper electrode and chamber are grounded. Gas flows are metered by mass flow controllers. To ensure good mixing, the gas passes through a mixing volume before entering the reactor through a showerhead in the upper electrode. Gases are then pumped in a radially uniform manner through the bottom of the reactor. Reactor pressure is monitored with a capacitance manometer, used in combination with a feedback control valve to maintain constant pressure. The reactor is equipped with quartz windows for optical access.

The lower electrode was powered by a 13.56 MHz power supply, coupled through a matching network equipped with an internal blocking capacitor. A shunt circuit,[10] consisting of a coil and an air-variable capacitor, was connected between the power lead and the chamber ground. At 13.56 MHz, the shunt has a net inductive impedance that cancels the net capacitive reactance of the rest of the cell, thereby reducing the total current drawn by the cell and improving the precision of current measurements.[11] On the power lead just upstream of the shunt, a Pearson model 2877 current probe[12] and a Phillips PM 8931 100:1 attenuating voltage

probe[12] were attached. An identical current probe was mounted on the short, solid copper wire that grounds the upper electrode to the exterior of the cell. Phase errors caused by propagation delays in the lines connecting the probes to the oscilloscope were measured and accounted for, within an error of $\pm 1°$. The measurement accuracy of current and voltage magnitudes is limited by the oscilloscope, which is rated at $\pm 3\%$. Using the probes and procedures described previously,[13] the stray impedance of the cell was characterized. This characterization allows us to convert the current and voltage wave forms at the measurement points into the current and voltage wave forms at the electrodes themselves. It also allows us to obtain the plasma impedance and the plasma power, which is the power delivered to the discharge itself, excluding all external power losses.

Measurements were made in 92% CF$_4$/O$_2$ and 50% C$_2$F$_6$/O$_2$ chamber-cleaning plasmas. (Percentages indicate mole percent.) Both gas mixtures were studied at pressures varying from 13.3 to 133.3 Pa (100–1000 mTorr) at 10 and 30 W of plasma power, corresponding to power densities of 0.12 and 0.37 W/cm^2, respectively. These power densities are comparable to industrial reactors operated at hundreds of watts because of the larger size of industrial reactors and the fact that external losses are usually not taken into account. Measurements were also made in 75% CF$_4$/Ar and 75% CF$_4$/10% O$_2$/Ar plasmas at 66.7 and 133.3 Pa (500 and 1000 mTorr) and 10 W of plasma power. The total gas flow rate was 9.5 sccm for CF$_4$/O$_2$ and C$_2$F$_6$/O$_2$, 10.6 sccm for CF$_4$/O$_2$/Ar, and 10.3 sccm for CF$_4$/Ar. For each condition, PLIF, emission and electrical measurements were made.

We performed PLIF to measure 2D CF$_2$ relative spatial density in the plasma as a chemical marker of plasma uniformity. The PLIF experimental apparatus is shown schematically in Fig. 1(b). The 266 nm laser beam from a quadrupled Nd:YAG laser was expanded using cylindrical optics into a vertical laser sheet approximately 2.5 cm tall and 0.5 cm thick. The laser sheet passes through the plasma, exciting the CF$_2$ radicals from the $X(0,1,0)$ ground electronic state to the $A(0,2,0)$ excited electronic state. The laser-excited CF$_2$ fluoresces primarily to the $X(0,0-20,0)$ states,[14] emitting light between 250 and 400 nm. The $X(0,8-20,0)$ $\leftarrow A(0,2,0)$ fluorescence between 300 and 400 nm was collected at a right angle to the direction of propagation of the laser beam, using an intensified charge-coupled device (ICCD) camera with a 105 mm, f/4.5 ultraviolet lens. Colored glass filters were used to reduce broadband plasma emission and to block the 266 nm scattered laser light. For each image, 1000 laser shots were averaged. In PLIF, only the CF$_2$ in the plane of the laser sheet is excited and detected, such that the image is not line-of-sight integrated. The spatial resolution was determined by the 5.0 mm laser sheet thickness and the 0.2 mm$\times$0.2 mm imaged dimensions of the camera pixels.

Broadband, spontaneous plasma emission from multiple species between 300 and 400 nm was measured and subtracted from the PLIF image. After each PLIF measurement,

an ICCD image of the broadband spontaneous plasma emission was acquired over the same total time as the PLIF image, but with the laser blocked. Because emission occurs throughout the plasma, the emission image, unlike the PLIF image, is a line-of-sight integrated measurement. After subtracting the plasma emission, the PLIF images were normalized for spatial variations and drift in the laser intensity. To measure the vertical profile of laser intensity, a 5% reflection was split off from the main laser sheet and was directed through a cuvette containing a dilute solution of Rhodamine 6 G laser dye in methanol. The laser sheet caused the dye to fluoresce with an intensity which was linearly proportional to the laser power, as verified using a laser power meter. A video CCD camera imaged the dye cuvette, simultaneously with the PLIF measurements, recording the vertical profile of laser intensity. In addition, a uniform field correction[15] was applied to the images to normalize for any slight variations in collection efficiency across the ICCD.

The normalized PLIF intensity is directly proportional to the electronic ground state density of CF_2, provided certain conditions are met. First, the CF_2 PLIF signal must be linear with laser power. This was found to be the case in the present experiments. Second, collisional quenching, which is the removal of excited state species due to collisional deexcitation or reaction, must not affect the fluorescence yield. This was verified by measuring the fluorescence decay time for both gas mixtures over the pressure range used in this study. In all cases, the fluorescence lifetime did not vary with pressure, and was found to be in excellent agreement with the published[14] fluorescence lifetime of 61 ± 3 ns. The conclusion that quenching is negligible is consistent with previous studies[7,16] and with quenching rate coefficients in the literature which have been measured for O_2,[17] CF_4,[18] and many other colliders.[17–20]

Third, the CF_2 rotational and vibrational population distribution must not vary with experimental conditions or position. For C_2F_6, CF_4, and CF_4/O_2 at pressures of 6.7–13.3 Pa and applied powers of 50–100 W, CF and CF_2 rotational temperatures of 325–400 K have been reported.[21,22] The CF_2 vibrational temperature measured in C_2F_6 at 13.3 Pa and 100 W applied power was 425 ± 25 K, which agreed to within experimental error with the measured CF_2 rotational temperature 400 K.[21] Translational temperatures, which are believed to be in equilibrium with CF_2 rotational temperature due to its long chemical lifetime,[23–25] have been obtained in CF_4 plasmas by CF_4 absorption linewidth measurements.[26,27] As the pressure increased from 3.33 to 23.3 Pa, the translational temperature increased from 318 to 360 K. As the applied power increased from 25 to 150 W at 26.6 Pa, the translational temperature increased from 312 to 345 K. Similarly, in C_2F_6 an increase in CF rotational temperature from 324 to 383 K was observed as the applied power increased from 50 to 100 W at 6.67 Pa.[22] Based on these previous studies, the temperatures for the experimental conditions in this study (pressures of 13.3–133 Pa and plasma powers of 10 and 30 W) are estimated to be within the range 325–400 K. To determine the effect of temperature changes on the

PLIF intensity, ground electronic state population fractions were calculated using partition functions, treating CF_2 as a prolate symmetric rotor[28] with molecular constants from Mathews,[29] and assuming that the rotational and vibrational temperatures were equal. As the temperature increases, an increase in $v_2'' = 1$ population is partially offset by a shift in rotational population out of the probed rotational levels, resulting in a 43% increase in the PLIF intensity for a temperature increase from 325 to 400 K. This must be kept in mind when comparing PLIF data from widely varying pressures or powers. For fixed experimental conditions, spatial variations in temperature are expected to be small. In a previous study, no significant spatial variation in temperature was detected in CHF_3 plasmas at 33.3 Pa.[26] In this study, temperature gradients are expected to be similarly small, except perhaps at the highest pressures where highly localized behavior is observed. Therefore spatial variations in PLIF intensity are attributed to changes in CF_2 density rather than to temperature effects.

III. RESULTS & DISCUSSION

A. PLIF results

Figures 2, 3, and 4 show 2D contour maps of CF_2 density as a function of pressure for three different plasma conditions: 92% CF_4/O_2 at 10 W, 92% CF_4/O_2 at 30 W and 50% C_2F_6/O_2 at 10 W, respectively. In each of the figures, three different regimes of behavior are observed. First, at low pressures of 13.3–26.7 Pa (100–200 mTorr), the CF_2 density is diffuse and is maximized near the outer edge of the electrodes, closer to the powered electrode. As pressure is increased, the CF_2 density increases and shifts closer to the center of the electrodes. At intermediate pressures of 53.3–80.0 Pa (400–600 mTorr), CF_2 at the center reaches its maximum density and is radially uniform across the electrode surface. As pressure increases still higher, the CF_2 density decreases in the region near the electrode center, but begins to increase in a localized region at the edge of the powered electrode. At the highest observed pressure of 133.3 Pa (1000 mTorr), the CF_2 density has contracted to a ring around the powered electrode edge. The transitions between regimes are gradual and occur at lower pressures in C_2F_6/O_2 than in CF_4/O_2. For 92% CF_4/O_2, the overall CF_2 density at 30 W in Fig. 3 is higher by about a factor of 2 than that at 10 W in Fig. 2. In 50% C_2F_6/O_2 at 10 W, the overall CF_2 density is lower than that in 92% CF_4/O_2 at 10 W by a factor which ranges from 1.3 to 4.7, depending on pressure. For 50% C_2F_6/O_2 at 30 W (not shown), the behavior is nearly identical to the 10 W data in Fig. 4, except that overall CF_4 density is higher by roughly a factor of 2.

To compare radial changes in CF_2 density for all pressures investigated, the CF_2 density was averaged axially and plotted versus radial position in Figs. 5(a) and 5(b). In 92% CF_4/O_2 at 10 W in Fig. 5(a), the three pressure regimes observed in Fig. 2 are visible. As pressure is increased from 13.3 to 66.7 Pa (100–500 mTorr), the CF_2 density increases at the radial center of the discharge and becomes more radi-
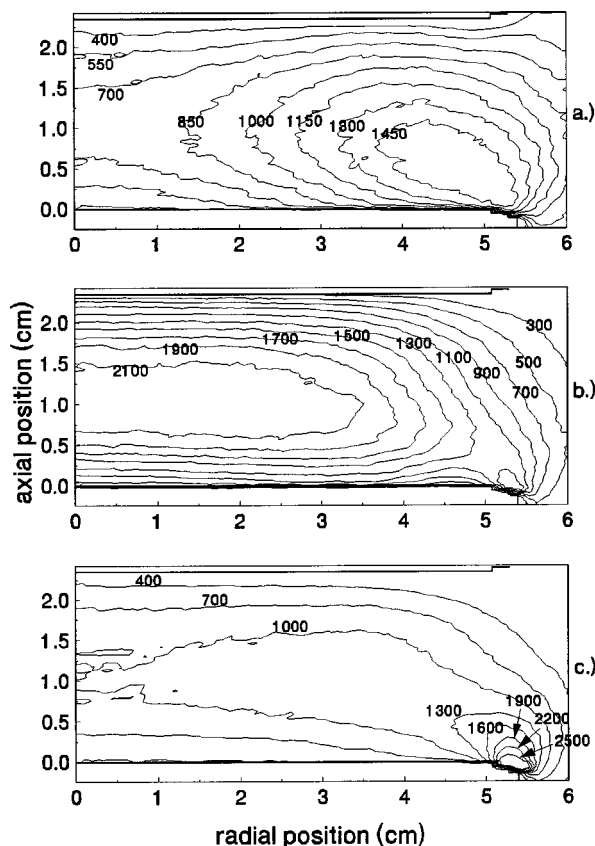
Fig. 2. 92% CF_4/O_2 CF_2 PLIF contour maps at 10 W and (a) 26.7 Pa (200 mTorr), (b) 80.0 Pa (600 mTorr), and (c) 133.3 Pa (1000 mTorr). Outlines of the upper (grounded) and lower (powered) electrodes are shown. Each contour map displays half of the plasma, such that the left side of the map shows the plasma center and the right side shows the electrode edge. All PLIF contour values in Figs. 2, 3, and 4 are normalized to the same intensity scale (in arbitrary units).
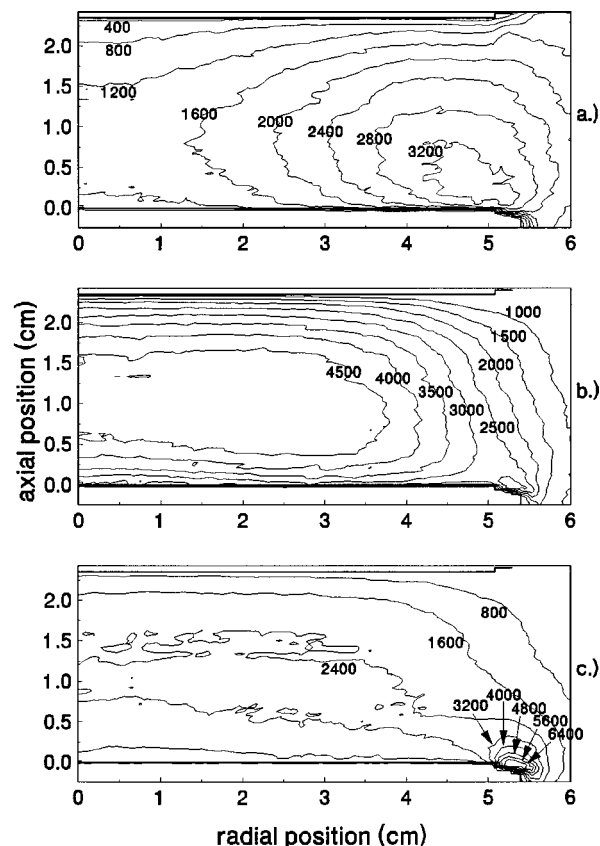
Fig. 3. 92% CF_4/O_2 CF_2 PLIF contour maps at 30 W and (a) 26.7 Pa (200 mTorr), (b) 80.0 Pa (600 mTorr), and (c) 133.3 Pa (1000 mTorr). Outlines of the upper (grounded) and lower (powered) electrodes are shown. Each contour map displays half of the plasma, such that the left side of the map shows the plasma center and the right side shows the electrode edge. All PLIF contour values in Figs. 2, 3 and 4 are normalized to the same intensity scale (in arbitrary units).

ally uniform. As pressure continues to increase up to 133.3 Pa (1000 mTorr), CF_2 density decreases at the radial center, while it increases in a very localized radial region at the electrode edge, where two peaks are observed. The inner peak occurs above the very edge of the electrode, while the outer peak is above the ground shield. For 50% C_2F_6/O_2 at 10 W, shown in Fig. 5(b), radial uniformity is achieved at a lower pressure of about 40 Pa (300 mTorr). Also, in Figure 5b the high pressure collapse and peak at the electrode edge is much more pronounced at 133.3 Pa (1000 mTorr) than it is for 92% CF_4/O_2 at 10 W in Fig. 5(a). For both CF_4/O_2 and C_2F_6/O_2, radial profiles of CF_2 density at 30 W are similar to the 10 W data.

To observe the change in CF_2 axial distribution with pressure, Fig. 5(c) shows CF_2 density along the axial centerline plotted versus axial position for 92% CF_4/O_2 at 10 W. CF_2 decreases noticeably at both the powered and grounded electrode. A decrease in CF_2 density near the electrodes due to surface losses has been noted in other studies.[23,30,31] The decrease at the powered electrode is less pronounced at the lowest pressures. For 92% CF_4/O_2 at 30 W, the axial profiles are very similar to Fig. 5(c). For 50% C_2F_6/O_2, the axial profiles are much flatter and the decrease at the electrodes is

less pronounced than for CF_4/O_2, especially at 30 W.

Previously, CF_2 PLIF measurements in CF_4, CF_4/Ar, and $CF_4/O_2/Ar$ plasmas were made by McMillin and Zachariah.[16] For comparison to their work, measurements were made at 66.7 and 133.3 Pa (500 and 1000 mTorr) in 10% $O_2/75\%$ CF_4/Ar and 75% CF_4/Ar, both at 10 W. In 10% $O_2/75\%$ CF_4/Ar at 10 W, we found that the CF_2 spatial distribution was the same as for 92% CF_4/O_2 at 10 W. Thus, the substitution of Ar for CF_4 made very little difference in CF_2 spatial uniformity, although the density of CF_2 was roughly a factor of 1.7 less in the Ar-containing mixture. Because McMillin and Zachariah[16] only studied the O_2-containing mixture at 66.7 Pa (500 mTorr), pressure dependence cannot be compared. Their CF_2 spatial distribution at 66.7 Pa (500 mTorr) exhibited uniformity across most of the electrode surface, consistent with our results. For 75% CF_4/Ar, we found the same behavior shown in Fig. 9(a) of McMillin and Zachariah; the image-averaged CF_2 density increased with pressure throughout the range studied. No collapse of the CF_4/Ar discharge was observed. A lowering in plasma electron density due to electron attachment by highly electronegative gases is believed to play a major role in the collapse.[3,5] Thus, because CF_4/Ar discharges are less
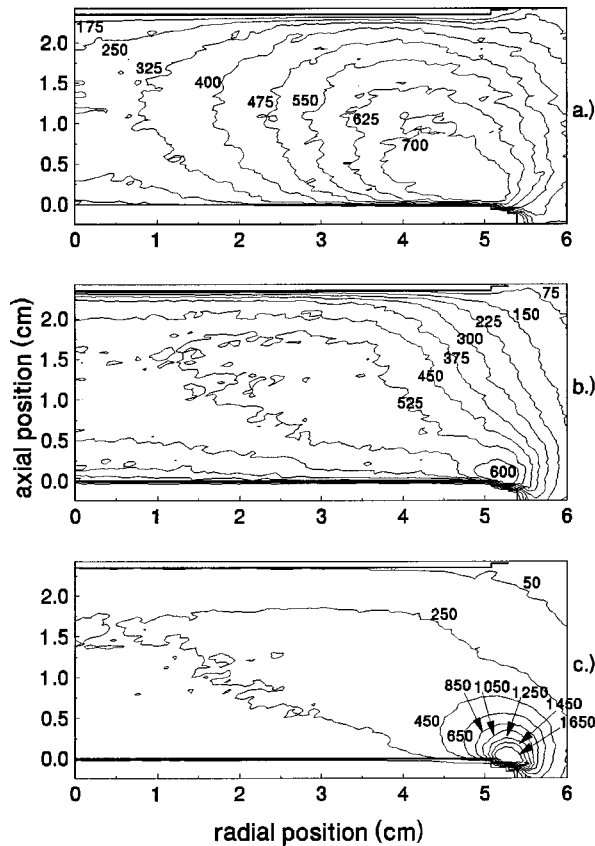
FIG. 4. 50% C$_2$F$_6$/O$_2$ CF$_2$ PLIF contour maps at 10 W and (a) 13.3 Pa (100 mTorr), (b) 53.3 Pa (400 mTorr) and (c) 120.0 Pa (900 mTorr). Outlines of the upper (grounded) and lower (powered) electrodes and ground shields are shown. Each contour map displays half of the plasma, such that the left side of the map shows the plasma center and the right side shows the electrode edge. All PLIF contour values in Figs. 2, 3 and 4 are normalized to the same intensity scale (in arbitrary units).

electronegative than O$_2$-containing discharges, the collapse of CF$_4$/Ar discharges should occur at higher pressures, if it occurs at all. Similarly, the collapse of 50% C$_2$F$_6$/O$_2$ discharges is observed at pressures lower than 92% CF$_4$/O$_2$ discharges, because the former is more electronegative. Extremely electronegative Ar/NF$_3$ plasmas are observed to collapse at even lower pressures.[5]

The CF$_2$ PLIF data provide insight into the relative cleaning rates at different cell surfaces. For example, one would expect the etch rate at the center of the powered electrode to be largest at intermediate pressures where the CF$_2$ density at $R=0$ and, presumably, the density of the active etchant species at $R=0$ are maximized, as seen around 66.7 Pa (500 mTorr) in Figs. 2(b), 3(b), 4(b), and 5. In contrast, at $R=6$ cm, a radial position far from the discharge center, the CF$_2$ density is maximized around 13.3–26.6 Pa (100–200 mTorr), as shown in Fig. 5(a) and 5(b). Thus, the etch rate at radially remote surfaces should be highest in the low pressure regime. In the ''collapsed plasma'' regime observed at the highest pressures, one would expect a very nonuniform etch rate with a strong peak at the edge of the powered electrode. Similar types of behavior appear to occur in commercial reactors,[2] where chamber cleaning is often accomplished
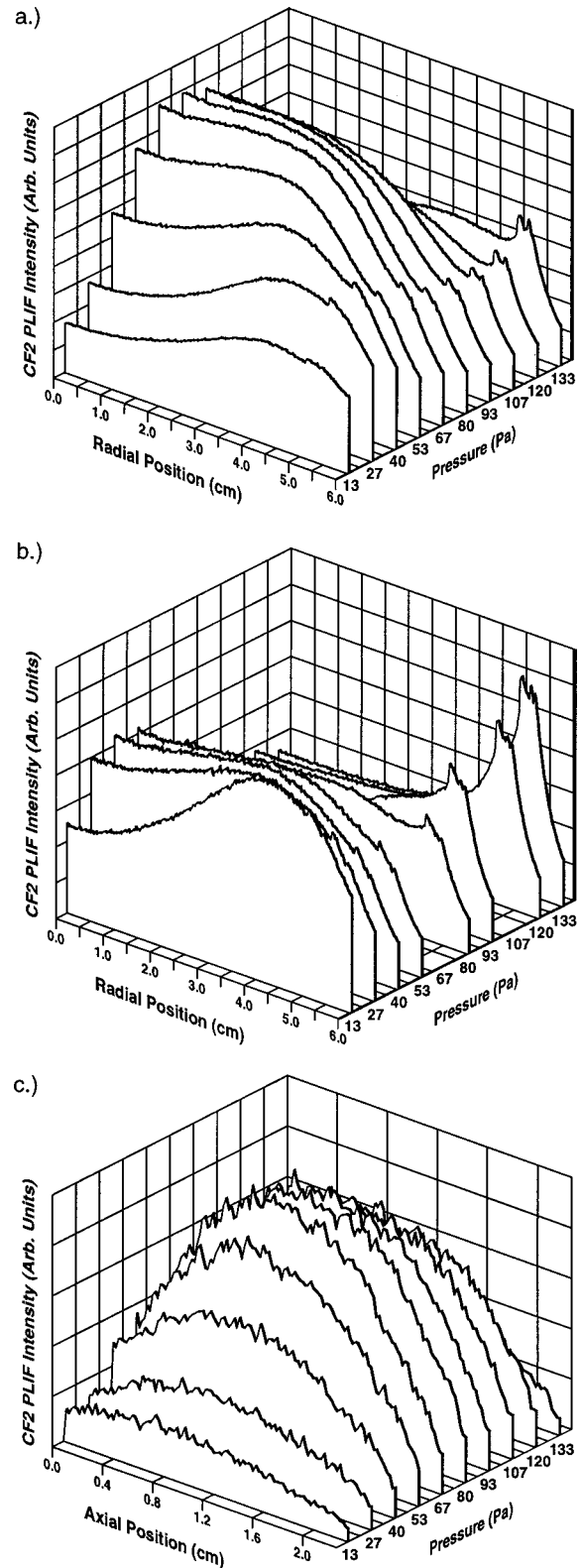

FIG. 5. CF$_2$ PLIF radial and axial profiles versus pressure: (a) CF$_2$ PLIF averaged axially and plotted vs radial position for 92% CF$_4$/O$_2$ at 10 W, (b) CF$_2$ PLIF averaged axially and plotted versus radial position for 50% C$_2$F$_6$/O$_2$ at 10 W. In the radial plots, the center of the electrodes are at zero, the electrode edge is at 5.1 cm, and the outer edge of the ground shield is at 5.4 cm. (c) CF$_2$ PLIF vs axial position along the vertical centerline for 92% CF$_4$/O$_2$ at 10 W. In the axial plot, the lower (powered) electrode is at zero and the upper (grounded) electrode is at 2.25 cm.

by two steps: one at lower pressure to clean the outer regions of the reactor, and one at somewhat higher pressure to clean the showerhead and susceptor area.

The association of high PLIF intensity with high etch rate assumes that in regions of high CF$_2$ density the density of F, believed to be the active etchant species, is also high. Although certain reactions[32,33] that produce CF$_2$ also produce F, one cannot assume that CF$_2$ and F densities will be perfectly correlated, because the plasma chemistry is quite complex. For example, CF$_2$ is consumed by O atoms to produce F atoms.[33] Nevertheless, at intermediate pressures where high CF$_2$ density was observed by PLIF, high F emission intensity has been observed.[5] Also, previous studies of NF$_3$/Ar, O$_2$/CF$_4$, and O$_2$/C$_2$F$_6$ chamber-cleaning plasmas in the GEC cell[3] and another reactor[4] showed that the etch rates of silicon nitride and silicon dioxide at the center of the powered electrode are highest at intermediate pressures. (The pressure at which maximum etch rate occurred increased with decreasing electronegativity of the gas mixture.) Furthermore, etch rates were correlated to optical emission and electrical parameters which will be shown below to be correlated to the PLIF results.

B. Emission results

Broadband plasma emission occurs from electron impact dissociation and electronic excitation of molecules in the plasma, resulting in electronically excited molecular fragments and atoms which subsequently emit. Thus, emission measurements give different information than CF$_2$ PLIF measurements, which detect CF$_2$ in its electronic ground state. The lifetimes of many of the created excited state fragments are very short (61 ± 3 ns (Ref. 14) for CF$_2[A\ ^1B_1(0,0,0)]$ and 26.7 ± 1.8 ns (Ref. 34) for CF$(A\ ^2\Sigma^+,v'=0)$) such that the fragments emit before they have a chance to travel away from the region in which they were created. Thus, the spatial distribution of the emission intensity indicates where reactive species, including CF$_2$, are created in the plasma. Once CF$_2$ emits and drops back down to the ground electronic state, it lives long enough[23,24] in the plasma to diffuse into other regions, where it can be detected using PLIF.

Figure 6 shows contour maps of emission emitted in the wavelength range of 300–400 nm for 92% CF$_4$/O$_2$ at 30 W. Emission occurs primarily near the powered (lower) electrode and near the grounded electrode, with less emission occurring in the bulk regions. The emission intensities near the grounded electrode and in the bulk of the plasma peak at intermediate pressures. The radial distribution of emission near the powered electrode varies with pressure: at low pressures [Fig. 6(a)] and high pressures [Fig. 6(c)] it is highest near the edge of the powered electrode, but at intermediate pressures [Fig. 6(b)] it is highest near $R=0$. Similar radial variations were observed for 50% C$_2$F$_6$/O$_2$ at 30 W. At 10 W, the highest emission intensities were observed near the outer edge of the powered electrode for both gas mixtures and all pressures. Overall emission intensity increased
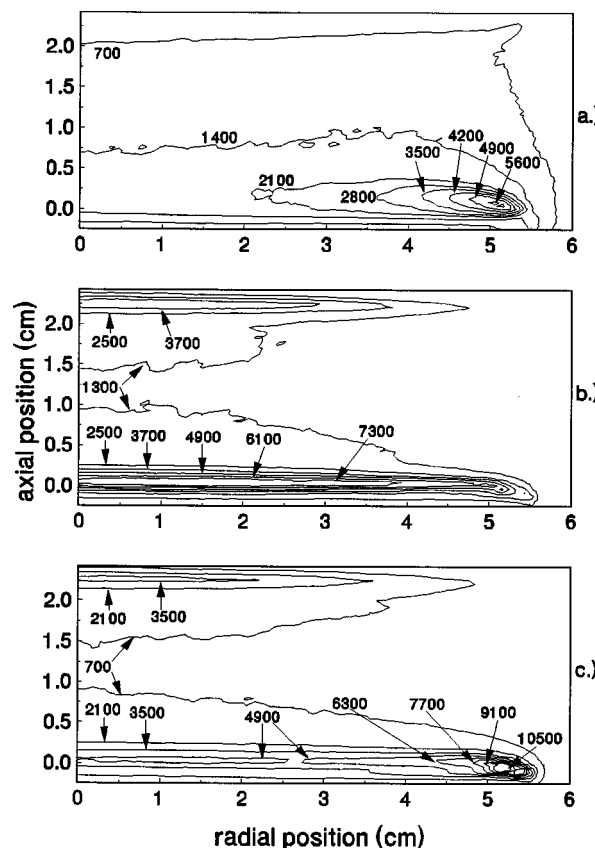

FIG. 6. 92% CF$_4$/O$_2$ emission contour maps at 30 W and (a) 26.7 Pa (200 mTorr), (b) 80.0 Pa (600 mTorr), and (c) 133.3 Pa (1000 mTorr). The electrodes are not shown. The lower (powered) electrode is at axial position=0, and the upper (grounded) electrode is at axial position=2.25 cm. Each contour map displays half of the plasma, such that the left side of the map shows the plasma center and the right side shows the electrode edge. All emission contour values in Fig. 6 are normalized to the same intensity scale (in arbitrary units).

strongly with power but varied little with changing gas mixture, as will be shown below.

Spatial changes in emission can be more readily observed by looking at axial and radial profiles, as shown in Figs. 7(a), 7(b), and 7(c). In Fig. 7(a), emission along the axial centerline of the image ($R=0$) is plotted as a function of pressure for 92% CF$_4$/O$_2$ at 30 W. Because emission is a ''line-of-sight'' measurement, the observed emission comes not only from the focal plane of the camera, but also from in front of and behind the focal plane. Therefore, the emission at $R=0$, shown in Fig. 7(a), is not necessarily from the radial center; rather it includes contributions from all the radial positions along the line-of-sight. In the axial profiles, as in the emission contour maps, most of the emission is observed to occur near the grounded (upper) or powered (lower) electrodes. The emission near either electrode initially increases with pressure, reaches a maximum at intermediate pressures and then falls off.

Figures 7(b) and 7(c) show emission versus radial distance. Because emission is primarily observed near the electrodes, it is desirable to show the emission intensity near the upper electrode and that near the grounded electrode inde-
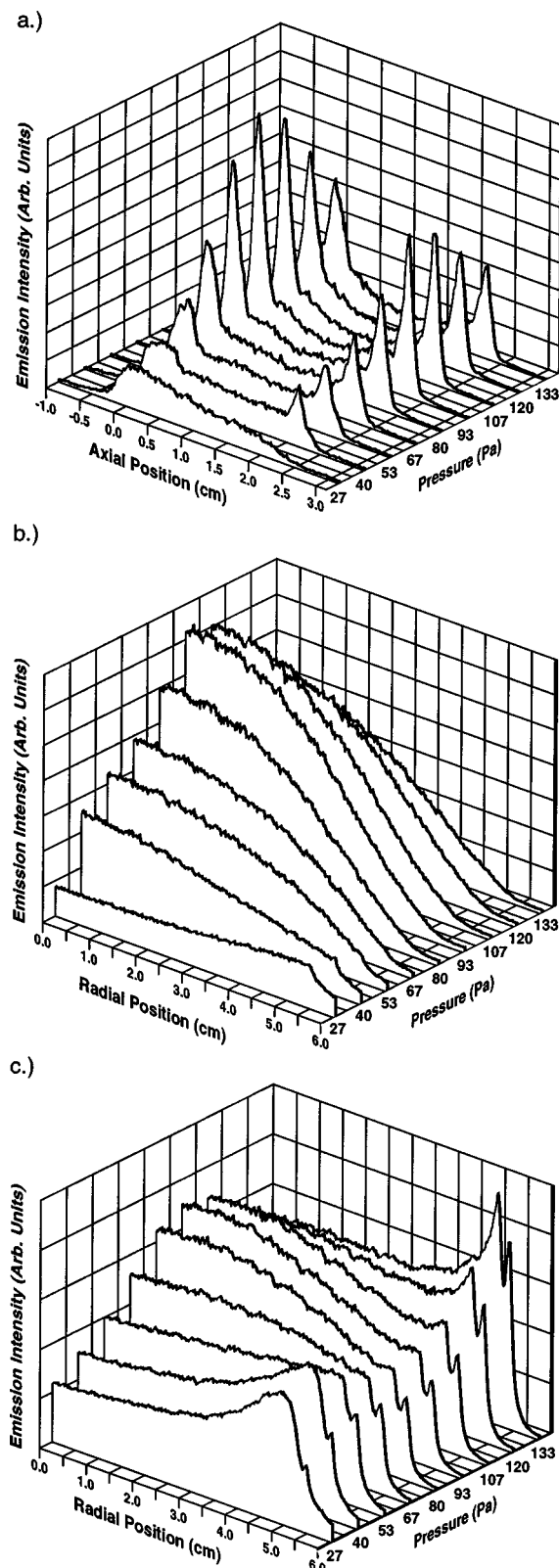
a.)

b.)

c.)

FIG. 7. Broadband emission axial and radial profiles vs pressure for 92% CF$_4$/O$_2$ at 30 W. (a) Emission intensity vs axial position along the vertical centerline. In the axial plot, the lower (powered) electrode is at zero and the upper (grounded) electrode is at 2.25 cm. (b) Emission intensity averaged over an axial distance near the upper (grounded) electrode and plotted vs radial position. (c) Emission intensity averaged over an axial distance near the lower (powered) electrode and plotted vs radial position. In the radial plots, the center of the electrodes are at zero, the electrode edge is at 5.1 cm, and the outer edge of the ground shield is at 5.4 cm.

pendently. Thus, emission was averaged separately over the axial distances (roughly 0.5 cm) near each electrode where emission peaked. The emission near the grounded electrode is shown in Fig. 7(b) for 92% CF$_4$/O$_2$ at 30 W. Because the emission is a ''line-of-sight'' measurement, it can be difficult to draw conclusions about the spatial distribution of the emission; however, qualitative conclusions can be drawn using general arguments. Emission generated uniformly over a ''disk-like'' region will result in a radial profile with a maximum at the axial centerline. Emission generated from a ''ring-like'' region should have a radial profile maximized near the electrode edges with a minimum at the axial centerline. At 26.7 Pa (200 mTorr), the emission appears ''ring-like,'' while above 26.7 Pa, the emission appears to be ''disk-like.'' At 120.0 and 133.3 Pa (900 and 1000 mTorr), the emission has begun to decrease, corresponding to the beginning of the collapse of the plasma, but the ''disk-like'' distribution is maintained. Similar behavior is observed for the other conditions investigated, although the emission begins to decrease at around 66.6 Pa (500 mTorr) for the C$_2$F$_6$/ O$_2$ mixtures.

Figure 7(c) shows the emission near the powered electrode versus radial distance for 92% CF$_4$/O$_2$ at 30 W. At low pressures, the emission occurs in a ''ring-like'' distribution near the electrode edge. As pressure increases, the emission becomes more uniform and ''disk-like'' across the electrode surface until the plasma begins to collapse at around 120.0–133.3 Pa (900–1000 mTorr). At this point, the emission near the center of the electrode decreases with pressure, and a double peak at the electrode edge becomes quite prominent. As with the emission near the grounded electrode, similar behavior is observed for both gas mixtures and both powers, except that the collapse is observed at lower pressures in the C$_2$F$_6$/O$_2$ mixtures.

In a prior study, F atom and Ar atom emission intensities were measured in CF$_4$/O$_2$/Ar, C$_2$F$_6$/O$_2$/Ar and NF$_3$/Ar plasmas at pressures between 6.7 and 266.6 Pa (50–2000 mTorr).[5] Although experimental differences prevent direct comparison of the pressures at which maxima in emission were observed, their results are consistent with this study. Under most conditions the emission intensities were maximized at intermediate pressures: 106.7 Pa (800 mTorr) for CF$_4$/O$_2$/Ar and 73.3 Pa (550 mTorr) for C$_2$F$_6$/O$_2$/Ar. In another study, measurements of F atom and Ar atom emission intensities in NF$_3$/Ar plasmas were found to be directly proportional to the etch rates of silicon nitride and silicon dioxide at the center of the powered electrode.[3] This suggests that the relative cleaning rates at different cell surfaces may be correlated to the spatially resolved optical emission measurements presented here.

C. Electrical results and comparisons

In a previous study,[5] the intensity of the atomic fluorine and argon optical emission from NF$_3$/Ar, CF$_4$/O$_2$/Ar and C$_2$F$_6$/O$_2$/Ar chamber-cleaning plasmas was found to correlate with several electrical parameters, and possible explanations were proposed to explain these correlations. The spa-
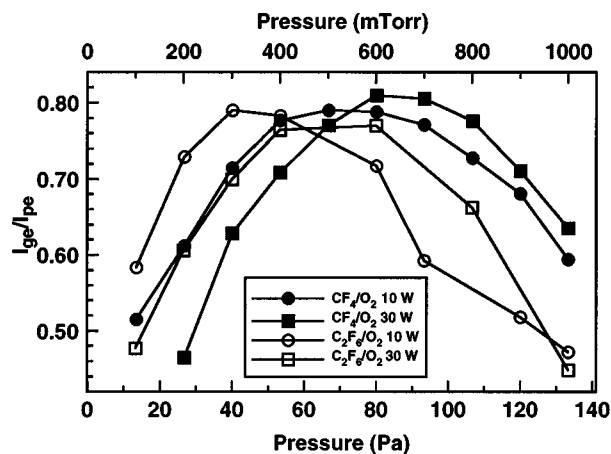
FIG. 8. Ratio of the fundamental (13.56 MHz) amplitudes of the currents at the grounded electrode (I_{ge}) and the powered electrode (I_{pe}) plotted vs pressure.
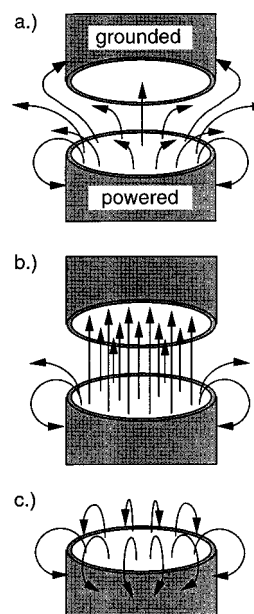

FIG. 9. Current flow diagrams for three regimes of operation in the GEC cell: (a) low pressure regime where current flows to the cell walls, (b) intermediate pressure regime where current flows primarily to the grounded electrode, and (c) high pressure regime, where current flows to ground shield around the powered electrode.

tially resolved optical measurements presented above have allowed us to further investigate such correlations. One particularly important electrical parameter identified in Ref. 5 is I_{ge}/I_{pe}: the ratio of the fundamental amplitude of the current at the grounded electrode to the fundamental amplitude of the current at the powered electrode. In Fig. 8, a plot of I_{ge}/I_{pe} versus pressure exhibits three different pressure regimes which parallel the three pressure regimes apparent in the emission and CF$_2$ PLIF measurements. First, there is a regime at low pressures where I_{ge}/I_{pe} is small, which coincides with the pressures at which CF$_2$ PLIF images show a broad maximum near the edge of the electrodes. In the second regime at intermediate pressures, I_{ge}/I_{pe} peaks, reaching a maximum of about 0.8. This regime coincides with the pressure range at which radially uniform CF$_2$ PLIF images were observed. Finally, in a third regime at high pressures, coinciding with the collapse of the plasma to a small ring near the edge of the powered electrode, I_{ge}/I_{pe} becomes small again.

One interpretation for the I_{ge}/I_{pe} data is illustrated in Fig. 9. The arrows shown in the figure represent the flow of rf current through the plasma and can be considered stream lines of the total current at a single instant of time. The current flowing into the plasma that does not flow to the grounded electrode must flow to some other reactor surface. None of the stream lines shown in the figure can terminate within the plasma, because the total current, which is the sum of the displacement current and the conduction current, has zero divergence. In the low pressure regime, depicted in Fig. 9(a), the current flows predominantly to the ground shields of both electrodes, and possibly out to the walls of the vacuum chamber as well. At these low pressures, the CF$_2$ PLIF, emission, and electrical characteristics of the chamber-cleaning plasmas resemble those of discharges in electropositive gases like argon. Computer simulations of argon discharges in the GEC cell show a distribution of current between the grounded surfaces which is quite similar to that shown in Fig. 9(a).[35] In contrast, at intermediate pressures, illustrated in Fig. 9(b), the more remote current paths shown

in Fig. 9(a) are less favored, and most of the current I_{pe} flows to the grounded electrode, as indicated by the maximum in I_{ge}/I_{pe} in Fig. 8. Finally, in the high pressure regime where the discharge collapses to a region very close to the edge of the powered electrode, most of the current presumably takes the very short path to the ground shield of the powered electrode, as shown in Fig. 9(c).

In this study, as in previous work,[5] the behavior of the current in Figs. 8 and 9 is further correlated to and explained by electrical impedance measurements. These are illustrated in Figs. 10(a) and 10(b), which plot the magnitude and phase of the impedance of the discharge Z_{pe}, as a function of pressure. The impedance Z_{pe} is a combination of a resistive impedance contributed by the plasma and a capacitive impedance contributed by the sheaths. At low pressures, the phase of Z_{pe} is strongly negative and its magnitude decreases with pressure, indicating that the capacitive impedance of the sheaths dominates the resistive impedance of the plasma. Under these conditions, rf current is able to flow widely through the plasma, even into rather remote regions of diffuse plasma, as shown in Fig. 9(a). The current is restricted only from extremely remote regions where the local plasma resistance, which increases as the plasma becomes more diffuse, becomes comparable to the local impedance of the sheath at adjacent grounded surfaces. In contrast, at high pressures, the phase of Z_{pe} is near 0° and its magnitude increases with pressure, which indicates that the resistance of the plasma is dominant. The increase in plasma resistance with pressure serves to restrict the flow of current to a smaller and smaller volume, as shown in Figs. 9(b) and 9(c). The peak in I_{ge}/I_{pe} seen in Fig. 8, which corresponds with the pattern of current flow seen in Fig. 9(b), occurs at pressures
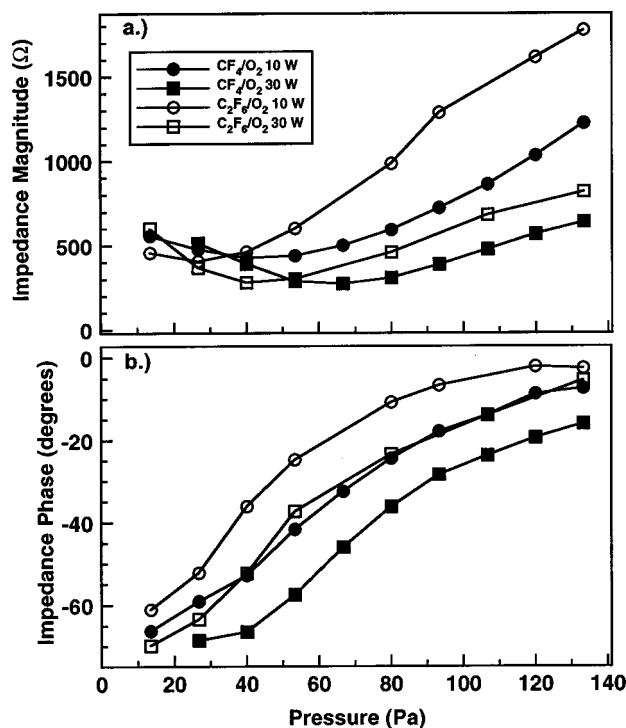
FIG. 10. Plots vs pressure for 92% CF$_4$/O$_2$ and 50% C$_2$F$_6$/O$_2$ at 10 and 30 W: (a) magnitude and (b) phase of Z_{pe}, the impedance of the discharge, defined as V_{pe}/I_{pe} where V_{pe} and I_{pe} are the fundamental (13.56 MHz) amplitudes of the voltage and current at the powered electrode.

FIG. 11. Plots vs pressure for 92% CF$_4$/O$_2$ and 50% C$_2$F$_6$/O$_2$ at 10 and 30 W: (a) I_{pe}(current flowing through powered electrode), (b) emission intensity averaged over the entire image, and (c) CF$_2$ PLIF intensity averaged over entire image. In (c) the C$_2$F$_6$/O$_2$ data have been multiplied by a factor of 5 to appear on a common scale with the CF$_4$/O$_2$ data. Within each plot of emission or CF$_2$ PLIF, the intensities have been normalized to the same intensity scale (in arbitrary units). The baseline indicates zero intensity.

close to and slightly above the minimum in Z_{pe}, when the phase of Z_{pe} is between $-30°$ and $-40°$. For either gas mixture, when the plasma power is increased from 10 to 30 W, the overall plasma density rises, decreasing the overall plasma resistance and shifting the impedance minimum and the peak in I_{ge}/I_{pe} to higher pressures, as explained in more detail in Ref. 5. Because C$_2$F$_6$/O$_2$ mixtures are more electronegative than CF$_4$/O$_2$, the C$_2$F$_6$/O$_2$ plasmas will have lower plasma densities and higher plasma resistances than CF$_4$/O$_2$ plasmas at any given pressure and plasma power. Therefore, for C$_2$F$_6$/O$_2$, the impedance minimum and the peak in I_{ge}/I_{pe} are shifted to lower pressures than for CF$_4$/O$_2$.

Optical emission is also correlated with current flow, because the mechanisms[36] that heat electrons, making emission possible, depend on the current density. Regardless of which mechanism is dominant (ohmic heating, stochastic heating, or heating of secondary electrons), variations in the rf current density at a surface, or along a surface, should result in variations in electron heating and concomitant variations in optical emission intensity. Consequently, the total current I_{pe}, plotted versus pressure in Fig. 11(a), displays a correlation with the total emission intensity averaged over the entire image, shown versus pressure in Fig. 11(b). In addition, the pressure dependence of the current at the grounded electrode I_{ge}, shown in Fig. 12(a), is correlated with the bulk emission intensity (the emission intensity at a small area centered both axially and radially) plotted versus pressure in Fig. 12(b).
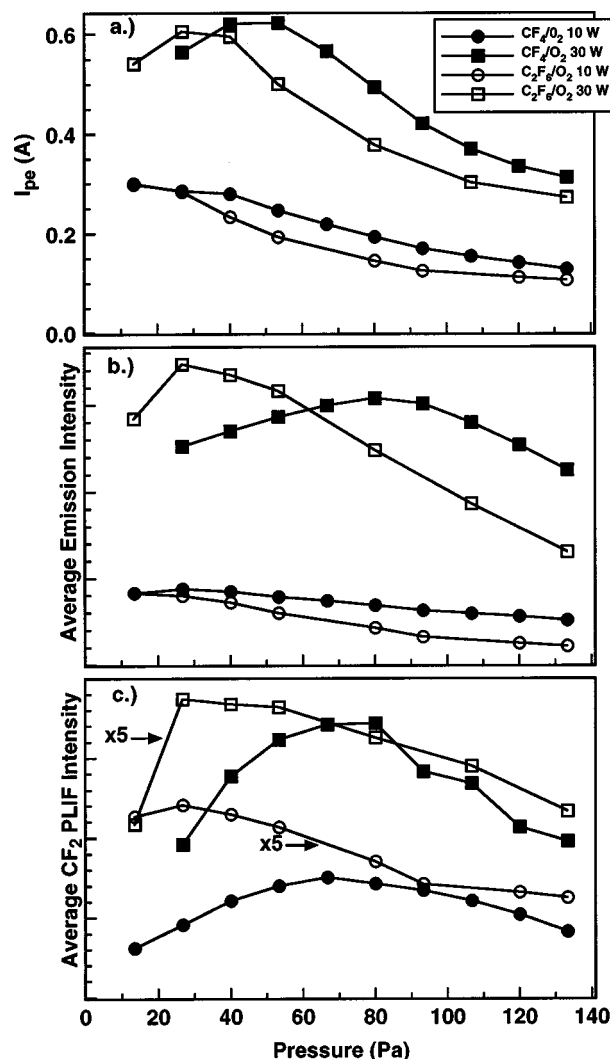
The correlations noted here are not perfect, perhaps because the electron heating mechanisms do not depend solely on the current density; rather, they also depend on other variables, such as the local electron density and electron temperature, which may vary independently with pressure.

The external electrical measurements do not provide any information about how the current density is distributed across the electrode surfaces. Nevertheless, some inferences can be made about the distribution of current density using the optical emission data, since the emitting species are created in areas of high current density. At intermediate pressures, when the radial emission profiles at the grounded or powered electrode in Figs. 7(b) and 7(c) are "disk-like," current should be fairly uniformly distributed across the electrode surfaces, as depicted in Fig. 9(b). In contrast, at lower
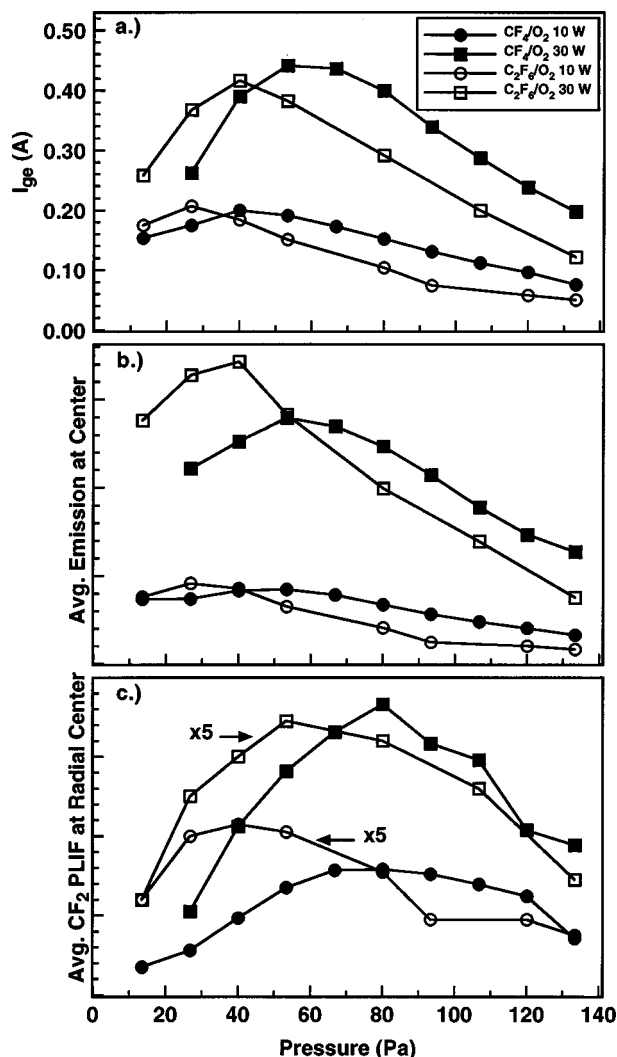
FIG. 12. Plots vs pressure for 92% CF$_4$/O$_2$ and 50% C$_2$F$_6$/O$_2$ at 10 and 30 W: (a) I_{ge}(current flowing through the grounded electrode), (b) emission intensity averaged over a small region at the radial and axial center, and (c) CF$_2$ PLIF averaged over the axial centerline. In (c), the C$_2$F$_6$/O$_2$ data have been multiplied by a factor of 5 to appear on a common scale with the CF$_4$/O$_2$ data. Within each plot of emission or CF$_2$ PLIF, the intensities have been normalized to the same intensity scale (in arbitrary units). The baseline indicates zero intensity.

or higher pressures, when the emission profiles are "ring-like," the current density should be more concentrated toward the outer edge of the electrodes, as shown in Figs. 9(a) and 9(c).

The total CF$_2$ PLIF intensity averaged over the whole image and the CF$_2$ PLIF intensity averaged over the axial center line are shown in Figs. 11(c) and 12(c), respectively. The total PLIF is somewhat correlated to the total emission signal in Fig. 11(b), presumably because the hot electrons that make emission possible are also responsible for the creation of CF$_2$. In contrast, the PLIF at the center is not as well correlated with emission at the center [Fig. 12(b)]. CF$_2$ observed at the radial center need not have been created at the center; it may have been created further out and then diffused inward. The PLIF at the center line is an important param-

eter, since it should correlate with the etch rate at the center of the electrodes, provided that the chemically reactive species responsible for the etching process is formed and transported in a manner similar to CF$_2$. The CF$_2$ PLIF at the center line is best correlated to the I_{ge}/I_{pe} data in Fig. 8 and the impedance data in Fig. 10: the pressures at which peaks occur in Fig. 12(c) correspond to the pressures where I_{ge}/I_{pe} is maximized, where Z_{pe} is minimized, and where the phase of Z_{pe} is between $-30°$ and $-40°$. This suggests that measurement of the electrical parameters I_{ge}/I_{pe} or Z_{pe} could be of use in optimizing and monitoring chamber-cleaning processes, especially those which are designed to clean the central portions of either electrode.

IV. CONCLUSIONS

The results presented here provide insight into the chamber-cleaning process and help explain cleaning rates previously measured at the center of the powered electrode.[3,4] Prior studies have indicated the importance of changes in the power coupling efficiency with pressure[3–5] and of global changes in the mechanisms of power deposition in the plasma with pressure.[5] In this work, spatially resolved optical measurements were used to investigate the changes in the spatial uniformity of chamber-cleaning plasmas with pressure, power and gas mixture. The optical measurements and accompanying electrical measurements help explain the observed variations in plasma uniformity, identify important spatial effects which should be included in computer simulations, and suggest new methods of monitoring and optimizing chamber-cleaning plasmas.

In this work, three pressure regimes were identified. At low pressures, where rf current primarily flows to the ground shields of both electrodes and possibly out to the vacuum chamber walls, the emission contour maps indicate that the reactive species are being primarily created in a thin "ring-like" region near the edge of the powered electrode. At these low pressures, the CF$_2$ PLIF contour maps show that diffusion of the long-lived CF$_2$ results in a diffuse "ring-like" distribution. In the intermediate pressure regime, most of the current flows through the plasma to the grounded electrode. In this regime, the emission shows that the creation of excited, reactive species is occurring in thin, radially-uniform, "disk-like" regions near both electrodes. The PLIF results show that the CF$_2$ diffuses, resulting in a radially-uniform CF$_2$ distribution. In the high pressure regime, the discharge collapses, and the current flows directly to the ground shield of the powered electrode. Here, the species creation primarily occurs in a "ring-like" region, closely confined near the edge of the powered electrode. The CF$_2$ density also primarily remains in this region at these higher pressures, where diffusion occurs more slowly.

Because reactive species are responsible for chamber cleaning, understanding the behavior of the uniformity of the reactive species densities can aid in the optimization of chamber-cleaning processes. In the intermediate pressure regime, the cleaning rate at the center of the powered electrode is maximized,[3,4] and the densities at the radial center are

maximized for CF$_2$ and presumably for the active etchant species. This regime corresponds to a maximum in I_{ge}/I_{pe}, the fraction of the current flowing to the grounded electrode, and a minimum in Z_{pe}, the magnitude of the plasma impedance. Electrical measurements of I_{ge}/I_{pe} and Z_{pe} could potentially be used to identify when the plasma is operating in this intermediate regime, which is desirable for cleaning in the central region of the reactor, which includes the susceptor and showerhead areas. The densities of CF$_2$, and presumably of the active etching species, vary widely throughout the plasma reactor under different pressure conditions. Thus, we would expect cleaning rates to be different at other reactor surfaces, where the rate has not been measured. Observations of the spatial characteristics of optical emission, in addition to the electrical measurements, could aid in identifying the conditions under which reactive species are created in other regions which require cleaning. Thus, the correlations observed here between the CF$_2$ PLIF, the optical emission and the electrical parameters suggest that emission or electrical measurements could be of use in optimizing and monitoring chamber-cleaning processes both at the center of the electrodes and at more remote surfaces.

The strong variations in the radial uniformity observed here illustrate the importance of spatial effects in electronegative plasmas. Computer simulations of electronegative plasmas often include only a single spatial dimension. Such simulations may be adequate for the intermediate pressure region, where optical emission and PLIF intensities are most radially uniform, and where the rf current flows mostly in the axial direction. The low pressure and high pressure regimes, however, do not appear to be amenable to 1D simulation. To predict the spatial distribution in these nonuniform regimes, and to predict the transitions between regimes, 2D codes[37] are needed. The data presented here, especially the PLIF results, provide a useful quantitative test necessary for validation of such models.

[1]J. Langan, P. Maroulis, and R. Ridgeway, Solid State Technol. **39**, 115 (1996).

[2]T. Streif, G. DePinto, S. Dunnigan, and A. Atherton, Semicond. Int. **20**, 129 (1997).

[3]J. G. Langan, S. W. Rynders, B. S. Felker, and S. E. Beck, J. Vac. Sci. Technol. A **16**, 2108 (1998).

[4]J. G. Langan, S. E. Beck, B. S. Felker, and S. W. Rynders, J. Appl. Phys. **79**, 3886 (1996).

[5]M. A. Sobolewski, J. G. Langan, and B. S. Felker, J. Vac. Sci. Technol. B **16**, 173 (1998).

[6]W. R. Entley, J. G. Langan, B. S. Felker, and M. A. Sobolewski (unpublished).

[7]S. Pang and S. R. J. Brueck, Mater. Res. Soc. Symp. Proc. **17**, 161 (1983).

[8]D. L. Flamm, Solid State Technol. **22**, 109 (1979).

[9]J. K. Olthoff and K. E. Greenberg, J. Res. Natl. Inst. Stand. Technol. **100**, 327 (1995).

[10]P. J. Hargis, Jr. *et al.*, Rev. Sci. Instrum. **65**, 140 (1994).

[11]M. A. Sobolewski, J. Vac. Sci. Technol. A **10**, 3550 (1992).

[12]Certain commercial equipment, or materials are identified in this article to specify adequately the experimental procedure. Such identification does not imply recommendation or endorsement by the National Institute of Standards and Technology, nor does it imply that the materials or equipment identified are necessarily the best available for the purpose.

[13]M. A. Sobolewski, IEEE Trans. Plasma Sci. **23**, 1006 (1995).

[14]D. S. King, P. K. Schenck, and J. C. Stephenson, J. Mol. Spectrosc. **78**, 1 (1979).

[15]B. K. McMillin and M. R. Zachariah, J. Appl. Phys. **77**, 1 (1995).

[16]B. K. McMillin and M. R. Zachariah, J. Vac. Sci. Technol. A **15**, 230 (1997).

[17]W. Hack and W. Langel, J. Phys. Chem. **87**, 3462 (1983).

[18]W. Hack and W. Langel, J. Photochem. **21**, 105 (1983).

[19]G. Dornhofer, W. Hack, and W. Langel, J. Phys. Chem. **87**, 3456 (1983).

[20]C. A. F. Johnson and H. J. Ross, J. Chem. Soc., Faraday Trans. 1 **74**, 2930 (1978).

[21]J. P. Booth, G. Cunge, F. Neuilly, and N. Sadeghi, Plasma Sources Sci. Technol. **7**, 423 (1998).

[22]J. P. Booth, G. Hancock, and N. D. Perry, Appl. Phys. Lett. **50**, 318 (1987).

[23]J. P. Booth, G. Hancock, N. D. Perry, and M. J. Toogood, J. Appl. Phys. **66**, 5251 (1989).

[24]S. G. Hansen, G. Luckman, and S. D. Colson, Appl. Phys. Lett. **53**, 1588 (1988).

[25]M. Haverlag, W. W. Stoffels, E. Stoffels, G. M. W. Kroesen, and F. J. de Hoog, J. Vac. Sci. Technol. A **14**, 384 (1996).

[26]M. Haverlag, E. Stoffels, W. W. Stoffels, G. M. W. Kroesen, and F. J. de Hoog, J. Vac. Sci. Technol. A **14**, 380 (1996).

[27]M. Haverlag, F. J. de Hoog, and G. M. W. Kroesen, J. Vac. Sci. Technol. A **9**, 327 (1991).

[28]J. P. Booth, D. Philos. thesis, Oxford University, 1988.

[29]C. W. Mathews, Can. J. Phys. **45**, 2355 (1967).

[30]J. P. Booth, G. Hancock, N. D. Perry, D. C. W. Blaikley, J. A. Cairns, and R. Smailes, Mater. Res. Soc. Symp. Proc. **98**, 135 (1987).

[31]J. W. J. Thoman, K. Suzuki, S. H. Kable, and J. I. Steinfeld, J. Appl. Phys. **60**, 2775 (1986).

[32]D. L. Flamm, J. Appl. Phys. **51**, 5688 (1980).

[33]I. C. Plumb and K. R. Ryan, Plasma Chem. Plasma Process. **6**, 205 (1986).

[34]J. P. Booth and G. Hancock, Chem. Phys. Lett. **150**, 457 (1988).

[35]S. Rauf and M. J. Kushner, J. Appl. Phys. **83**, 5087 (1998).

[36]M. A. Lieberman and A. J. Lichtenberg, *Principles of Plasma Discharges and Materials Processing* (Wiley, New York, 1994).

[37]S. Rauf and M. J. Kushner, J. Appl. Phys. **82**, 2805 (1997).